

Laminar Fluid Flow with Complex Material Behavior in Devices of Mechanical Engineering

Olaf Wünsch

University of Kassel, Department of Mechanical Engineering
Institute of Mechanics, Mönchebergstr 7, 34125 Kassel, Germany
wuensch@uni-kassel.de

ABSTRACT

The paper deals with the numerical simulation of highly viscous, non-Newtonian fluids in apparatus of mechanical engineering. Differential constitutive equations are used to approximate real material behavior of technical fluids such as polymer melts. The models consider shear-thinning viscosities, normal stress differences and other elastic properties which affect the fluid flow. Some details of the basis of the numerical simulations are discussed. The influence of the viscoelastic behavior is demonstrated through examples of flow calculations for two and three dimensional geometries. Comparison of the present results with other experimental and numerical results from the literature shows good agreement.

Keywords: non-Newtonian fluids, Giesekus fluid, Phan-Thien-Tanner model, square pipe flow, twin screw extruder

1. INTRODUCTION

In many branches of processing engineering, highly viscous liquids have to be transported in continuous operations. Heavy oils conveyed inside of pipes in chemical engineering and the transportation of nourishments in the food industry are prominent examples. Also, polymer melts, paints, effluents and cosmetics are some of the fluids with dense material behavior which is very different from that of low molecular liquids like water. Many of the latest fluids with low viscosities can be described by a Newtonian ansatz of friction under normal process conditions, where the viscosity is only a function of the temperature and the stress is connected linearly with the deformation. But for highly viscous materials it is possible to observe flow effects that cannot be explained by a model of a Newtonian fluid [1, 2]. One of these unusual behaviors is the Weissenberg effect. In contrast to a Newtonian fluid, a macromolecular liquid with free surface climbs to a stirrer in an agitator, if rotating at low speed. At the opening of a nozzle can be observed a die swelling by pressing a highly viscous fluid, before the cross section of the fluid is compressed by the inertia with growing distance. Another non-Newtonian effect is the elasticity: a fluid can be sucked out of an open vessel by using a pipe which only dips into the fluid at the beginning. Then the pipe can be lifted out without breaking the fluid filament. Finally many highly viscous fluids show shear-thinning behavior, where the viscosity decreases with increasing deformation. This paper throw light on the recent developments in the areas of highly viscous fluid flow and makes a brief review of some of the specific examples of challenging problems.

The analysis of flow problems in devices of mechanical engineering with highly viscous non-Newtonian fluids is a multidisciplinary field of research – the engineers model the fluid flow and formulate the required equations, the chemists analyze the material behavior and the mathematicians are needed to find fast and convergent solutions to the equations. In addition, different scales in time and space complicate the solution of the flow problems. In order to confine the field of analysis we define the Reynolds number,

$$\text{Re} = \frac{\rho U L}{\eta} \ll 1, \quad (1)$$

where, ρ denotes the fluid density, U and L a characteristic velocity and length, respectively. Usually the viscosities of non-Newtonian fluids are very high, so the Reynolds number tends

towards zero. In comparison with the friction, the inertia can be neglected (creeping flow conditions).

This paper gives an overview of the methods to analyze the flow of distinct viscoelastic fluids. First, we introduce the basic equations in order to calculate the pressure and velocity field in complex, three-dimensional geometries. By way of example, we use two differential material equations to approximate the behavior of the fluid under steady conditions. Numerical methods are needed to solve the generated coupled system of differential equations. Some remarks explain the implementation into a commercial software package. Some numerical results for two- and three- dimensional fluid flows are given to demonstrate the influence of viscoelasticity.

2. ANALYSIS OF THE TRANSPORT MECHANISM

2.1 Basic Equations

We confine our analysis to isothermal problems, so the basis for description of laminar, highly viscous and incompressible fluids is the conservation of mass and momentum which read in differential formulation [3]

$$\operatorname{div} \mathbf{v} = 0, \quad (2)$$

$$\rho \left(\frac{\partial \mathbf{v}}{\partial t} + (\operatorname{grad} \mathbf{v}) \mathbf{v} \right) = -\operatorname{grad} p + \operatorname{div} \mathbf{T} + \mathbf{f}. \quad (3)$$

were ρ is the density of the fluid, \mathbf{v} the velocity vector, p the pressure, \mathbf{T} the extra stress tensor and \mathbf{f} the vector of volume forces like gravity. To describe the material behavior of the complex fluids it is possible to use two types of constitutive equations for the extra stress tensor [4] – the differential or the integral formulation, which both have pros and cons. The integral constitutive equations are able to fit real complex material data in a very good manner [1], but it is complicated to implement the equations into numerical codes [5]. Differential equations are easier to program, but they only partially fit the material data.

In order to calculate three-dimensional fluid flow in devices of mechanical engineering with numerical methods, we use a differential formulation which reads

$$\mathbf{T} + \lambda_1 \left[(1 - \xi) \overset{\nabla}{\mathbf{T}} + \xi \overset{\Delta}{\mathbf{T}} \right] + \mathbf{B}(\mathbf{T}) = 2\eta \left(\mathbf{D} + \lambda_2 \overset{\nabla}{\mathbf{D}} \right). \quad (4)$$

\mathbf{D} is the rate of deformation tensor, $\overset{\Delta}{\mathbf{T}}$ and $\overset{\nabla}{\mathbf{T}}$ denote the covariant and contravariant time derivatives of the extra stress tensor

$$\overset{\Delta}{\mathbf{T}} = \frac{D\mathbf{T}}{Dt} + \mathbf{L}^T \cdot \mathbf{T} + \mathbf{T} \cdot \mathbf{L} \quad (5a)$$

$$\overset{\nabla}{\mathbf{T}} = \frac{D\mathbf{T}}{Dt} - \mathbf{L} \cdot \mathbf{T} - \mathbf{T} \cdot \mathbf{L}^T, \quad (5b)$$

were $\mathbf{L} = \operatorname{grad} \mathbf{v}$ denotes the velocity gradient tensor and

$$\frac{D\mathbf{T}}{Dt} = \frac{\partial \mathbf{T}}{\partial t} + (\operatorname{grad} \mathbf{T}) \mathbf{v} \quad (6)$$

represents the material derivative with respect to time, \mathbf{D} is the rate of deformation tensor and $\mathbf{B}(\mathbf{T})$ denotes an additional material function in dependence of the symmetrically extra stress tensor \mathbf{T} . The material constants $\lambda_1, \lambda_2, \eta, \xi$ of the model are used to fit rheological data of measurements of real fluids. In the case of $\mathbf{B}(\mathbf{T}) = 0$, Eq. (4) leads to an Oldroyd-4-constant model. Various other material

equations with $\mathbf{B}(\mathbf{T}) \neq 0$ are reported in literature. In the following, we use two models, the Giesekus model [6]

$$\mathbf{B}(\mathbf{T}) = \alpha \frac{\lambda_1}{\eta} \mathbf{T} \cdot \mathbf{T}, \quad \text{with } 0 \leq \alpha \leq 1, \xi = 0, \lambda_2 = 0, \quad (7)$$

and the Phan-Thien-Tanner model [7]

$$\mathbf{B}(\mathbf{T}) = \alpha \frac{\varepsilon \lambda_1}{\eta} \text{tr}(\mathbf{T}) \mathbf{T}, \quad \text{with } \alpha > 0, \xi = 0, \lambda_2 = 0. \quad (8)$$

Both material equations show similar behavior at shear and elongation flow – the shear viscosity decreases with higher shear rate (shear thinning behavior), the normal stress coefficients [8]

$$v_1 = \frac{\sigma_{xx} - \sigma_{yy}}{\dot{\gamma}^2}, \quad v_2 = \frac{\sigma_{yy} - \sigma_{zz}}{\dot{\gamma}^2}$$

decrease monotonically with increasing shear rates and the elongational viscosity grows with the strain. Figure 1 shows dependence of the normalized material functions for a Giesekus model on the normalized shear rate and strain rate, respectively [4]. This behavior is typical of many viscoelastic fluids such as polymer melts. The difference between the Phan-Thien-Tanner model and the Giesekus model is found in their gradients of decreasing viscosity and normal stresses at higher shear rates.

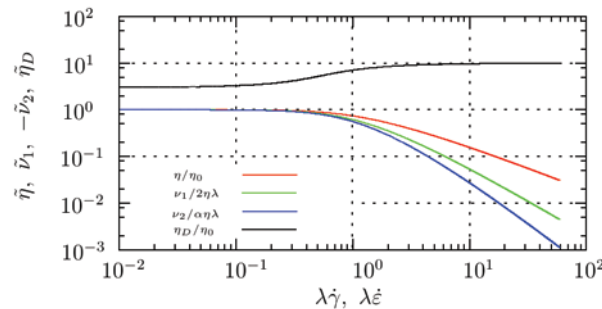


Figure 1. Normalized material functions of the Giesekus model: shear-thinning behavior of the shear viscosity (red), increasing elongation viscosity (black) and shear dependence of normal stress coefficients (green and blue).

In order to quantify the influence of the viscoelastic behavior of the fluid, we introduce the dimensionless Deborah number

$$De = \frac{\lambda_1}{t_p}, \quad (9)$$

which can be read as the ratio of material time to a typical process time. With increasing Deborah number the viscoelasticity gains prominence, while the limit $De \rightarrow 0$ represents a Newtonian fluid.

2.2 Numerical Implementation

Equations (2) through (4) are a coupled system of differential equations which have to be solved simultaneously in order to calculate the fluid flow in devices of mechanical engineering. Because of the nonlinear material behavior and the complex geometries, a finite volume method is used to solve the equations. This numerical treatment is a standard technique in calculating such fluid flows. Of many commercial and noncommercial software packages that are available in the

market, we have acquired considerable experience of using FLUENT [9] which is a popular software for solving flow problems. The standard version is not able to calculate using viscoelastic material equations, so we use the software interface to implement our own user defined functions. First, we split the stress tensor in the momentum equation into a Newtonian and a non-Newtonian part [10],

$$\mathbf{T} = \underbrace{2\eta_{new}}_{\tau^{new}} \mathbf{D} + \mathbf{T}^{non-new} \quad (10)$$

The non-Newtonian stresses are calculated using the Giesekus or Phan-Thien-Tanner model. Then a further parameter

$$\beta = \frac{\eta_{new}}{\eta_{new} + \eta}, \quad (11)$$

appears, which quantifies the ratio of Newtonian and non-Newtonian stresses. In detailed notation, Eq. (4) is a system of three independent (planar flow) or six independent (three-dimensional flow) scalar differential equation for the stress components. We can rewrite the expression for each component to form a transport equation. For example, using the Giesekus model in the case of a 2-D flow, a normal stress reads

$$\lambda_1 \left(\frac{\partial \tau_{xx}}{\partial t} + u \frac{\partial \tau_{xx}}{\partial x} + v \frac{\partial \tau_{xx}}{\partial y} \right) = 2\eta \frac{\partial u}{\partial x} - \tau_{xx} + 2\lambda_1 \left(\tau_{xx} \frac{\partial u}{\partial x} + \tau_{xy} \frac{\partial u}{\partial y} - \frac{\alpha}{2\eta} (\tau_{xx}^2 + \tau_{xy}^2) \right). \quad (12)$$

The left side of Eq. (12) denotes the material derivative of the transported extra stress component and the right side corresponds to the source term. Such equations can be defined as user functions in commercial software. In order to simulate the fluid flow by using the finite volume method the coupled differential system is solved with a standard iteration loop (SIMPLE). In each step, first the stress components are solved with the velocity field of the previous step and, subsequently, the momentum and mass equations are calculated.

The absence of diffusive terms in transport equations such as Eq. (12) requires some numerical arrangements. We use a strong under-relaxation parameter for the pressure, velocities and the stress components inside the SIMPLE iteration loop and discretize the space by second-order approximation. Even for stationary flow problems we calculate time-dependent until the flow cease to change and then apply the double precision version of the software.

3. RESULTS

3.1 Planar Flow

In order to demonstrate the influence of the viscoelastic material behavior we present some results of numerical simulations for planar flow.

3.1.1 Flow of a 4-to-1 Contraction

One of the most used benchmark test in literature for numerical simulation of Newtonian and non-Newtonian fluids is the 4:1 contraction. A fluid with high viscosity flows through a planar channel and the size is changed abruptly in a 4-to-1 ratio, see Figure 2. The channel lengths are sufficiently long ($L_1/H_2 = 40$, $L_2/H_2 = 100$) so that the entrance and the exit of the channel do not influence the flow at contraction. For the simulation we construct a structured mesh with 135000 finite volumes. The following boundary conditions are used: the fluid adheres to all walls, fully developed flow at the entrance and outflow conditions at the exit.

Our results for fixed values of the Reynolds number and the non-Newtonian parameter ($\beta = 1/9$, $\varepsilon = 1/4$) are presented below. Only the Deborah number, which is calculated with the mean velocity at the outlet and smaller channel height,

$$De = \frac{\lambda_1 \bar{U}_2}{H_2},$$

is changed during different calculations. It is well known that in the case of Newtonian fluid a vortex exists at the concave corner and that its size is fixed for a given flow rate. However, in the case of a non-Newtonian fluid, with increasing Deborah number the vortex size increases and the center of the vortex moves down as shown in Figure 3. For $De = 10$ the vortex occupies the whole corner. These results seem to compare well with those from experiments performed by Boger and Walters [11], who investigated the vortex growth for creeping flow in a 4-to-1 circular contraction for a Boger fluid as shown in Figure 4. The similarity between depictions of the fluid flow behavior by the numerical and the experimental results is quite remarkable.

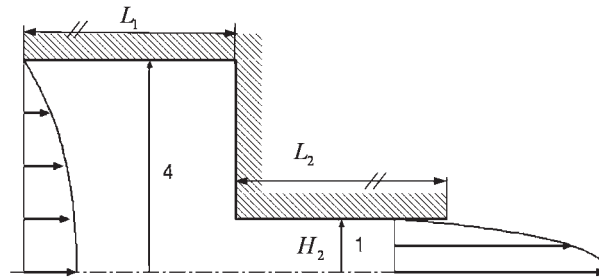


Figure 2. Sketch of the 4:1 contraction.

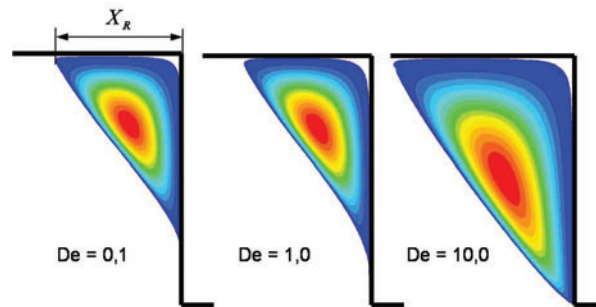


Figure 3. Influence of the Deborah number on corner vortex size.

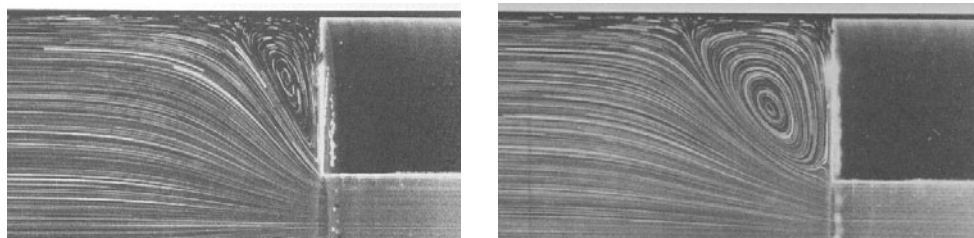


Figure 4. Experimental results for a Boger fluid (polyacrylamide in water and corn syrup solution) from [11]. From left to right: increase of the vortex size with increasing De number.

Details of extra stress tensor for $De = 10$ are presented in Figure 5. The extreme values of the extra stress components are reached near the lower convex corner.

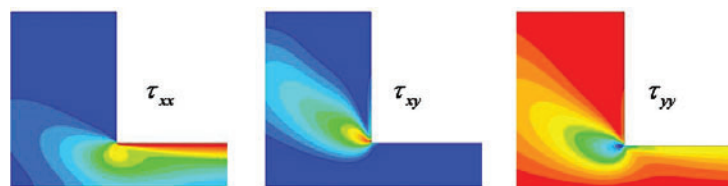


Figure 5. Components of the extra stress tensor for $De = 10$.

We validated our numerical results against the calculations made by Alves et al [12] for the flow of Oldroyd-B and PTT fluids in planar contraction, and found them comparing very closely with each other. Table 1 lists the length of the vortex (see Figure 3), the maximum of the normal stress component and the maximum of the velocity component in x-direction located at the centerline (dimensionless). The differences in the values are noted to be less than 2.5 % for X_R and less than 0.4 % for the flow parameters.

It is interesting to note the non-monotonic development of the maximum of extra stress and velocity at the centerline with the Deborah number (see Table 1). The length of the vortex grows with increasing Deborah number, but around $De = 1.0$ the normal stress reaches a maximum, whereas the velocity is at a minimum. This behavior is confirmed by the numerical results in [12]. Such unusual characteristic flow behavior is attributed to the nonlinear viscoelasticity.

Table 1: Comparison of the present calculations (normalized) with that due to Alves et al. [12]

	$\frac{X_R}{H_2}$	$\tau_{xx,max} \frac{H_2}{(\eta_{new} + \eta)\bar{U}_2}$ (centerline)	$\frac{u_{max}}{\bar{U}_2}$ (centerline)
Alves et al. [12], De = 10.0	2.131	0.264	1.531
Present calculation, De = 10.0	2.181	0.263	1.528
Present calculation, De = 1.0	1.565	0.402	1.480
Present calculation, De = 0.1	1.500	0.338	1.522

The flow behavior and the development of the vortex in the corner depend highly on the chosen material equation [13]. When the Oldroyd-B model was used, a second lip vortex was found to develop at the lower edge in the domain of $De = 2.0$ [14]. This behavior was not seen for the Phan-Thien-Tanner model. Hence, in order to simulate flow problems with viscoelastic fluids in a realistic way, it is essential to determine the material behavior exactly and choose the right model.

3.1.2 Flow over a Square Hole

The geometry of a planar channel with a square hole is investigated to quantify the disturbance of a fully developed channel flow. In analogy to the 4-to-1 contraction we expect a vortex in the hole, which depends on the material behavior of the fluid. Figure 6 shows the geometry used. The distance of the square hole to the upper wall of the channel is the same as the dimension of the hole. In order to ensure fully developed inlet and outlet flow, the channel lengths are 10 times the hole dimension. The structured mesh consists of 25000 cells with a refinement in the region around the hole. As in the case of 4-to-1 contraction, the fluid adheres to all fixed walls. At the inlet the velocity is given and at the outlet the pressure is fixed.

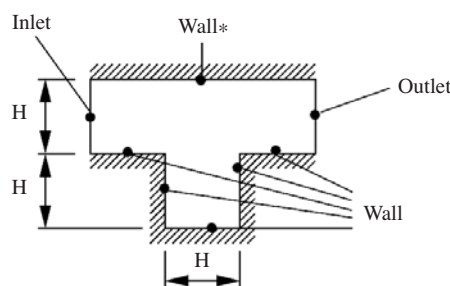


Figure 6. Geometry of a planar channel with a square hole.

Some numerical results for creeping flow ($Re = 0.01$) are given in Figure 7. It shows the streamlines for the flow, which moves over the hole from left to right. For the calculation we have used a Phan-Thien-Tanner model with a non-Newtonian parameter of $\beta = 0.5$. As expected, a vortex develops inside

the hole. For a Newtonian fluid the maximum depth of indentation is 25% of the length H and it is located at the centerline. The flow and all stresses are symmetrical. With increasing Deborah number the flow becomes asymmetric. The center of the vortex moves in the direction of the flow and the depth of indentation grows. Table 2 gives the normalized location of the depth and the vortex center as a function of the Deborah number.

Up to $De = 1$, the changes are continuous and the calculated flow does not depend on the time. With higher Deborah numbers, however, the flow behavior changes intermittently and the results can be time dependent [15, 16]. We observe that the vortex splits into two parts whose centers are on the opposite sides of the central plane of the hole. One of the time-dependent solutions is shown in Figure 7 (e).

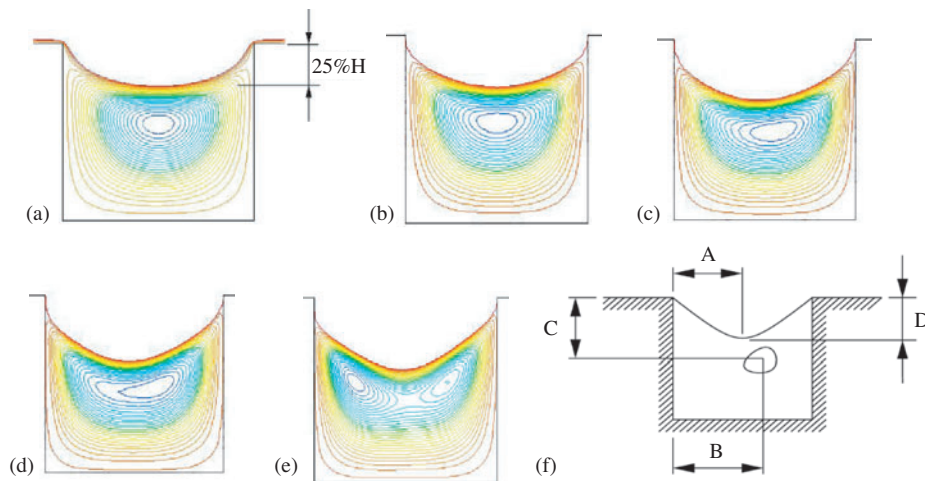


Figure 7. Streamlines inside the hole under creeping flow conditions ($Re=0.01$): (a) Newtonian fluid; (b) $De = 0.1$, $\varepsilon = 0.25$; (c) $De = 0.5$, $\varepsilon = 0.25$; (d) $De = 1.0$, $\varepsilon = 0.25$; (e) $De = 5.0$, $\varepsilon = 0.25$; (f) definition sketch of location of vortex center and depth of indentation.

Table 2: Normalized location of vortex center and depth of indentation as a function of Deborah number

De	A/H	B/H	C/H	D/H
0.01	0.500	0.501	0.459	0.278
0.1	0.480	0.512	0.479	0.291
0.5	0.462	0.570	0.510	0.323
1.0	0.458	0.624	0.522	0.373

3.2 Three-Dimensional Flow

Real devices of mechanical engineering are three dimensional, so it is necessary to appropriately adapt the numerical simulation. In this case, the stress tensor consists of 6 independent values, and for each stress component a differential transport equation has to be solved. Along with the 3 momentum equations and the mass balance a system of 10 coupled differential equations is generated.

3.2.1 Square Pipe Flow

In order to test the three-dimensional calculations we investigate the fully developed creeping flow in a square pipe [17]. Figure 8 shows a sketch of the pipe. A flow in such geometry is not really three dimensional. The vector of the velocity consists of three components which only depend on two coordinates that are perpendicular to the mean flow direction. For our calculation we take a volume domain which exists on the cross section and a small size in the third direction. Considering the symmetry of the cross section we only mesh a quarter (one of the quadrants as shown in Figure 8) by using 7500 structured finite volumes. For the boundary conditions we postulate no slip condition at the walls and symmetry about the lines of symmetry. Inlet and outlet of the volume domain are connected periodically. The flow is powered by a given pressure gradient.

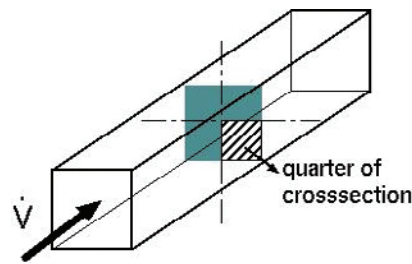


Figure 8. Sketch of the flow through a square pipe.

In the case of a fully developed Newtonian fluid flow only one velocity component in the flow direction exists, which depends on the cross coordinates. In contrast, the use of a viscoelastic material changes the flow behavior causing a secondary flow to develop in the cross section. Figure 9 shows the results of the calculation using a Phan-Thien-Tanner model at $De = 0.05$. Two vortices with different directions of rotation are observed in the quarter of the cross section. Colors are used to mark the magnitude of the velocity vector: blue for small velocities, and red for high velocities. The vortices are symmetrical about the diagonal line which divides the quarter in two eighth parts. The secondary flow is very slow. Compared with the maximum of the axial velocity the values are about 1000 times smaller.

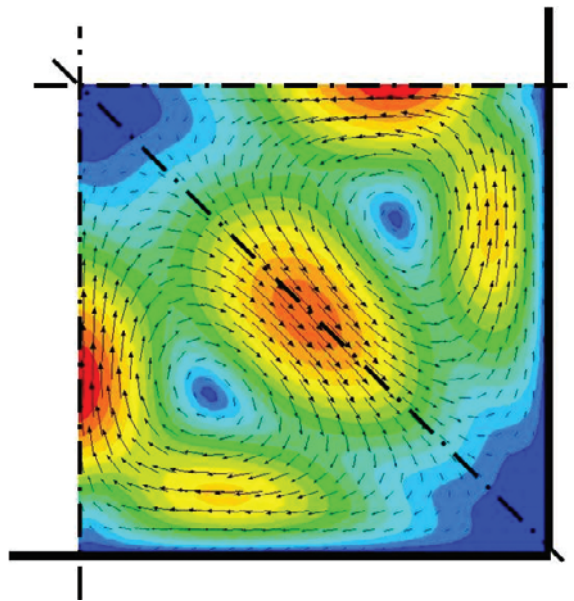


Figure 9. Velocity vectors in the quarter cross section: Viscoelastic Phan-Thien-Tanner model.

As a result of viscoelastic fluid flow the interaction between the secondary flow in the transverse plane (cross section) and the primary flow in the axial direction leads to helical curved path lines of material points. Further calculations with different material equations show that the rotating direction depends on the model and material constants used. Analytical investigations using a perturbation technique validate these observations [1]. The reason for evolution of the secondary flow is the difference in normal stresses.

3.2.2 Flow in a Twin Screw Extruder

Screw extruders are used in the process industry in different areas [18, 19]. The main task of such devices is conveying highly viscous or viscoplastic materials against a pressure gradient [20]. The extrusion of half-finished polymer products and injection molding are examples of screw extruder applications [21]. However, screw extruders also perform conditioning operations such as devolatilization of solvents and mixing of different components [22].

In order to design processes with screw extruders, it is necessary to know the flow conditions inside the machine. The quality of polymer products depends on the time of residence and on the strain during the extrusion. The geometry, material behavior and the process conditions are essential parameters to control the quality. In practice it is better to use twin-screw extruders than single-screw machines, especially for high flow capacity, mixing problems and tasks where self cleaning screws are necessary [23].

A picture of a typical twin screw extruder is shown in Figure 10. An electrical drive (left) powers two contra-rotating screws (speed n) inside a cylindrical barrel (right) and conveys the polymer melt through a special tool at the end of the extruder. The flights are built intermeshed and the surface of the screws is designed as kinematically self cleaning. The key parameters of the geometry are the diameter of the barrel d , the distance of the axis of the two screws, the pitch T , the number of threads Z and the tolerance between the screws and the barrel.

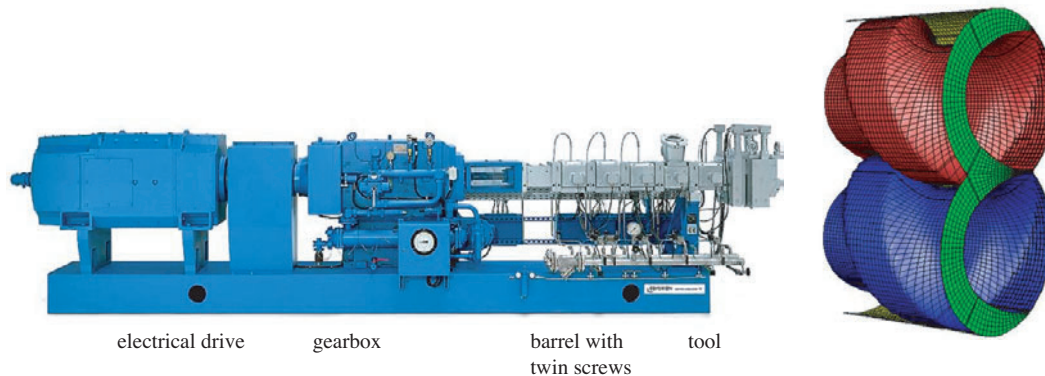


Figure 10. Design of a typical twin screw extruder (left) and sketch of the twin screw inside a cylindrical barrel (right).

In order to calculate the flow of a highly viscous fluid we postulate the following conditions: the screw extruder works horizontally and is fully filled, the fluid adheres to all walls and the flow is fully developed. In a fixed inertial system the velocity and pressure fields depend on the position and on the time. But in an observed system which moves along the extruder at the velocity Tn , the flow is stationary. What is more, the flow is periodical with “wave length” T/Z [24]. Therefore it is possible to confine the calculation domain in axial direction seen in Figure 10 (right) and inlet/outlet are coupled periodically.

Users of screw extruders are interested in the flow-rate and input-power-characteristics that depend on the geometry and material behavior. In order to reduce the number of independent parameters it is expedient to use dimensionless values. In addition to the Reynolds number, we introduce a pressure-parameter, a flow-rate-parameter and a power-parameter [22, 25]:

$$\text{Re} = \frac{\rho n d^2}{\eta}, \quad \text{K} = \frac{\Delta p d}{\eta_0 n T}, \quad \text{Q} = \frac{\dot{V}}{n d^3}, \quad \text{Pi} = \frac{P}{\eta n^2 T d^2}.$$

In order to quantify the characteristics that depend on a viscoelastic material we calculate the velocity and pressure fields numerically. The structured three-dimensional mesh is very fine and consists of more than 700,000 finite volumes. We apply the Giesekus model with the following dimensionless parameters,

$$\beta = 0.1, \alpha = 0.2, \text{De} = \lambda_1 n = 0.1,$$

where the Newtonian stresses represent only 10% of the non-Newtonian values. In comparison to the viscoelastic calculations, we simulate the flow using two additional material equations: a nonlinear viscous material equation (Cross model), which is able to approximate the shear-thinning behavior of the viscosity only,

$$\frac{\eta}{\eta_0} = \frac{1}{(1 + \lambda \dot{\gamma})^c},$$

where η_0 denotes the zero shear viscosity at low shear rates and c is a parameter to control the decrease of the viscosity at high shear rates; and a Newtonian fluid with constant viscosity η_0 . Some results of the simulations are shown in Figure 11. The pressure gradient depends on the flow-rate parameter. It is well known that the correlation between K and Q is linear in the case of Newtonian fluid and creeping flow. With increasing shear-thinning behavior (Cross model) the curve becomes non-linear and the ability of the screw extruder to work against a pressure gradient decreases. The viscoelastic Giesekus model shows the similar behavior, the two curves are close to each other. Obviously the same shear-thinning behavior of both models influences only the flow characteristic. Elastic properties such as normal stress differences or elongational viscosity are of no importance. It is notable that all curves coincide at the working point without pressure gradient ($K = 0$). Here the flow inside the extruder is very close to a pure shear flow where the non-Newtonian properties do not influence the velocity field.

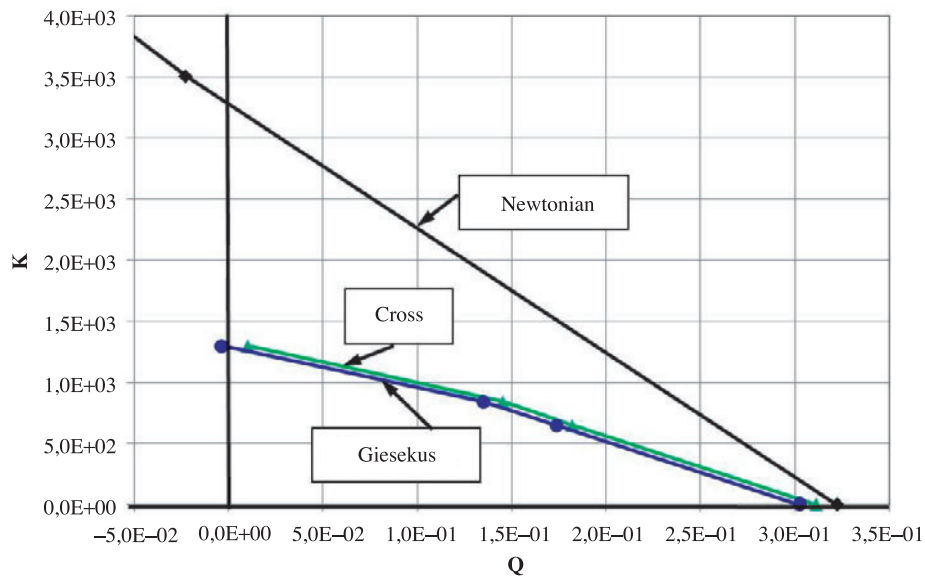


Figure 11. Flow characteristics of a twin screw extruder for Newtonian, shear-thinning (Cross) and viscoelastic fluid (Giesekus).

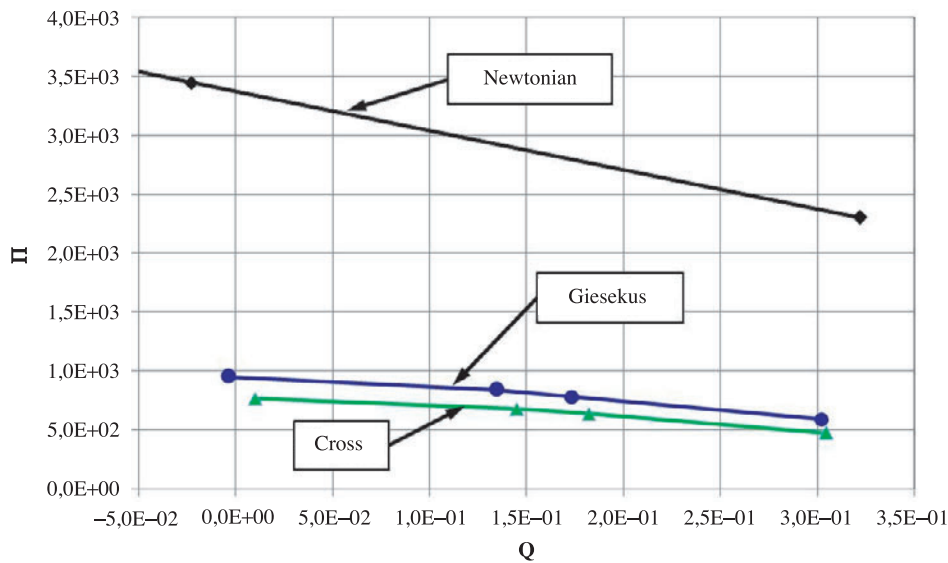


Figure 12. Power characteristics of a twin screw extruder for Newtonian, shear-thinning (Cross) and viscoelastic fluid (Giesekus).

The behavior of the power characteristic is similar to the flow characteristic, see Figure 12. Because of the shear-thinning viscosity the required drive power is only around 30% of the value for constant viscosity. The differences between the Cross model and the Giesekus model are only slightly greater than those of the flow characteristic.

More differences appear when viewing the distribution of the normal stress. By way of example, Figure 13 shows the component τ_{xx} in a cross section for different working points (left/right). For the Cross model (top) a symmetrical line for the stress distribution at both working points is observed. The same symmetry can be seen for Newtonian fluids. It is different for the Giesekus model (bottom). The viscoelasticity breaks the symmetry not only for the normal stresses but also for the shear stresses. This leads to a change in the force loading due to pressure and stresses at the screws and the barrel which results in a diversification of the abrasion.

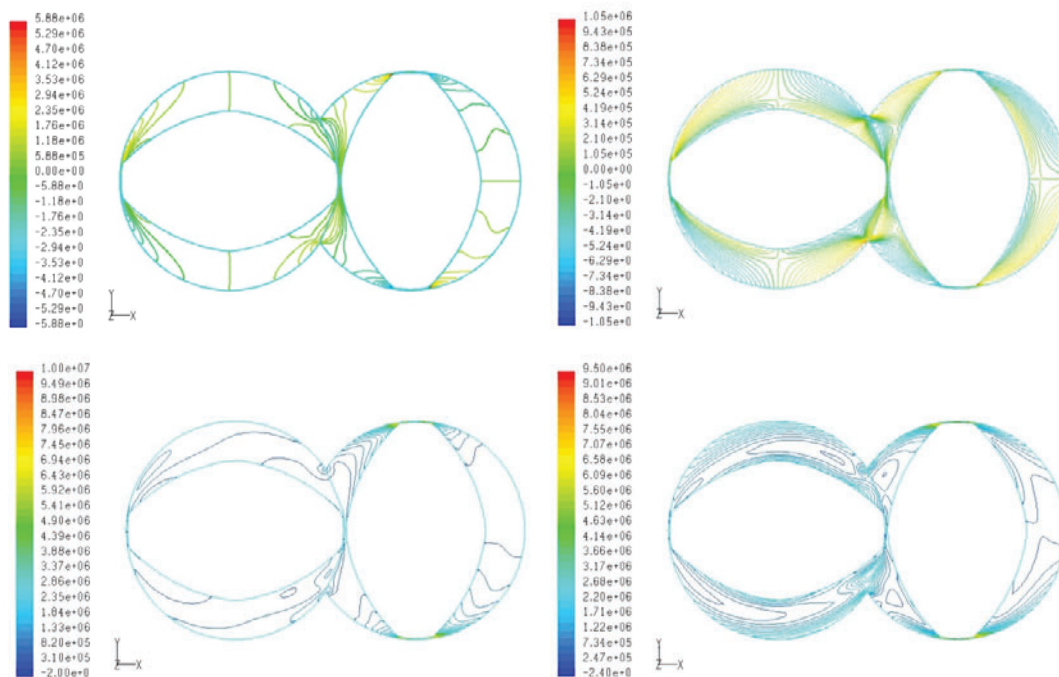


Figure 13. Isolines of the normal stress component in the cross section. Above: Cross model (only shear-thinning), below: Giesekus model (viscoelastic). Left: working point without pressure gradient ($K = 0$), right: working point without net flow ($Q = 0$).

4. CONCLUSION

The viscoelasticity is responsible for many flow phenomena which are not observed in Newtonian or pure nonlinear viscous fluids. The expansions of vortices and the development of secondary flows are effects resulting from differences in normal stresses in the case of stationary flow. Whether the viscoelasticity influences the fluid flow depends on the flow behavior. In pure shear flow the velocity field is determined by the moved walls only. The non-Newtonian forces do not begin to work until a pressure gradient works. This was shown by the Poiseuille flow conditions like the 4-to-1 contraction and the square pipe flow.

In order to configure flow apparatus and predict the flow rates in devices of mechanical engineering it is necessary to consider the right material behavior. Numerical simulations based on finite volume or finite element methods with commercial and noncommercial software are a good means of modeling the real fluid flow. Calculations with non-linear shear thinning viscosity are state-of-the-art, but more and more fluid viscoelasticity can be implemented in appropriate programs. Best experiences are made with material functions in differential form because they can be imported into standard solvers.

The choice of the right material equation is very important for getting the real fluid flow. Small differences in the material formulation can change the velocity field in a substantial manner. Therefore it is necessary to measure the material parameter of the fluid as much as possible and as accurately as possible as well as adapting all of them to given or newly developed material equations. This is one of the future tasks along with developing fast and converging algorithms to solve the coupled differential equations system.

ACKNOWLEDGEMENT

The author would like to thank A. Al-Baldawi, K. Khani and M. Krebs for the execution of the numerical simulations. The project is partially funded by the German Research Foundation (SFB/TR TRR 30).

REFERENCES

- [1] Böhme, G., *Strömungsmechanik newtonscher Fluide*, B.G. Teubner, Stuttgart, 2000
- [2] Dealy, J.M. and Larson, R.G., *Structure and rheology of molten polymers*, Hanser Publisher, Munich, 2006
- [3] Wünsch, O., *Strömungsmechanik des laminaren Mischens*, Springer-Verlag, Berlin, 2001
- [4] Bird, R.B., Armstrong, R.C. and Hassager, O., *Dynamics of polymeric liquids, Vol.1: Fluid mechanics*, J. Wiley & Sons, New York, 1987
- [5] Broszeit, J., Finite-element simulation of circulating steady flow for fluids of the memory-integral type: Flow in a single-screw extruder, *J. Non-Newt. Fluid. Mech.*, 1997, 70, 35–58
- [6] Giesekus, H.W., *Phänomenologische Rheologie*, Springer Verlag, Berlin, 1994
- [7] Xue, S.-C., Phan-Thien, N. and Tanner, R.I., Three dimensional numerical simulations of viscoelastic flows through planar contractions, *J. Non-Newt. Fluid Mech.*, 1998, 74, 195–245
- [8] Schowalter, W.R., *Mechanics of Non-Newtonian Fluids*, Pergamon press, 1978
- [9] FLUENT Flow modeling software. *ANSYS Germany GmbH, Darmstadt*
- [10] Rajagopalan, D., Armstrong, R.C. and Brown, R.A.: Finite element method for calculation of steady, viscoelastic flow using constitutive equations with a Newtonian viscosity. *J. Non-Newt. Fluid Mech.*, 1990, 36, 159–192
- [11] Boger, D.V. and Walters, K., *Rheological Phenomena in Focus*, Elsevier, Amsterdam, 1993
- [12] Alves, M.A., Oliveira, P.J. and Pinho, F.T., Benchmark solution for the flow of Oldroyd-B and PTT fluids in planar contraction, *J. Non-Newt. Fluid Mech.*, 2003, 110, 45–75
- [13] Hulsen, M.A., Fattal, R. and Kupferman, R., Flow of viscoelastic fluids past a cylinder at high Weissenberg number: Stabilized simulation using matrix logarithms, *J. Non-Newt. Fluid Mech.*, 2005, 127, 27–39
- [14] Damanik, H., Hron, J., Ouazzi, A. and Turek, S., Finite element discretization and newton-multigrid solution techniques for log-confirmation reformulation (LCR) for viscoelastic flow problems, *J. Non-Newt. Fluid Mech.*, 2009, submitted
- [15] Ellero, M. and Tanner, R.I., SPH-simulations of transient viscoelastic flows at low Reynolds number, *J. Non-Newt. Fluid Mech.* 2005, 132, 61–72
- [16] Xue, S.-C., Tanner, R.I. and Phan-Thien, N., Numerical modeling of transient viscoelastic flows. *J. Non-Newt. Fluid Mech.*, 2004, 123, 33–58
- [17] Wünsch, O. and Krebs, M., Numerical simulation of flow of viscoelastic fluids. *Proc. Appl. Math. Mech.*, 2007, 7, 4100021–4100022
- [18] Oswald, T.A., *Polymer processing*. Hanser Publishers, Munich, 1998
- [19] Oswald, T.A., Turng, L.-S. and Gramann, P.J., *Injection molding handbook*, Hanser Publisher, Munich, 2002
- [20] Böhme, G. and Broszeit, J., Numerical flow simulation for Bingham plastics in a single-screw extruder. *Theo. Comp. Fluid Dynamic*, 1997, 9, 65–74
- [21] Rees, H., *Molt engineering*, Hanser Publisher, Munich, 2002
- [22] Wünsch, O., Simulation von Mischvorgängen in Schneckenmaschinen, *Technische Mechanik* 1998, 18, 1–10

- [23] Kohlgrüber, K., ed., *Co-rotating twin-screw extruders*. Carl Hanser Verlag, Munich, 2008
- [24] Böhme, G. and Wünsch, O., Analysis of shear-thinning fluid flow in intermeshing twin screw extruders. *Arch. Appl. Mech.*, 1997, 67, 167–178
- [25] Wünsch, O., Kühn, R. and Heidemeyer, P., Simulation of the fluid flow of deeper screw flights for co-rotating twin screw extruders, *Proceed. Ann. Tech. Conf. ANTEC 2003*, Nashville, TN, USA, 338–343

